# Effects of spatial configuration of imperviousness and green infrastructure networks on hydrologic response in a residential sewershed

Theodore C Lim[1], Claire Welty[2]

[1] Penn Institute for Urban Research, University of Pennsylvania, Philadelphia, Pennsylvania, USA

[2] Center for Urban Environmental Research and Education and Department of Chemical, Biochemical, and Environmental Engineering, University of Maryland, Baltimore County, Maryland, USA

Corresponding Author: Theodore Lim, tlim@upenn.edu

## KEY POINTS

- A coupled hydrologic model was applied to simulate hydrologic processes in a medium density, residential sewershed
- Effects of nine spatial configurations of imperviousness and green infrastructure networks were tested and compared to monitored flow data
- Green infrastructure configurations in higher flow-accumulation areas were shown to intercept the most runoff



Suggested citation:
Lim, Theodore C., and Claire Welty. 2017. “Effects of Spatial Configuration of Imperviousness and Green Infrastructure Networks on Hydrologic Response in a Residential Sewershed.” Water Resources Research 53 (9): 8084–8104. https://doi.org/10.1002/2017WR020631.

## ABSTRACT

Green infrastructure (GI) is an approach to stormwater management that promotes natural processes of infiltration and evapotranspiration, reducing surface runoff to conventional stormwater drainage infrastructure. As more urban areas incorporate GI into their stormwater management plans, greater understanding is needed on the effects of spatial configuration of GI networks on hydrological performance, especially in the context of potential subsurface and lateral interactions between distributed facilities. In this research, we apply a three-dimensional, coupled surface-subsurface, land-atmosphere model, ParFlow.CLM, to a residential urban sewershed in Washington DC that was retrofitted with a network of GI installations between 2009 and 2015. The model was used to test nine additional GI and imperviousness spatial network configurations for the site and was compared with monitored pipe-flow data. Results from the simulations show that GI located in higher flow-accumulation areas of the site intercepted more surface runoff, even during wetter and multi-day events. However, a comparison of the differences between scenarios and levels of variation and noise in monitored data suggests that the differences would only be detectable between the most and least optimal GI/imperviousness configurations.

## KEYWORDS

Green Infrastructure, Stormwater Management, Imperviousness, Spatial Configuration, Urban Hydrology, ParFlow.CLM

# 1 INTRODUCTION

To date, hydrological modeling of urbanized watersheds has focused primarily on land cover and surface type. Impervious surface area has emerged has emerged as the dominant explanation for reduction of subsurface storage in urbanized watersheds [*Schueler*, 1994; *Arnold and Gibbons*, 1996; *Moglen and Kim*, 2007]. However, impervious surface area may not be the dominant explanation for changes in the urban hydrological cycle [*Bhaskar et al.*, 2015; *Smith et al.*, 2015; *Lim*, 2016]. Subsurface dynamics, inter-event capacity recovery through evapotranspiration from vegetation and potential interactions between overland flow and the differential contraction of saturated areas, and lower than expected hydraulic conductivity of urban soils are offered as possible explanations for changes in the hydrological cycle associated with urbanization. Most urban hydrological models do not account for context-dependent variation in soil permeabilities affected by antecedent wetting and groundwater flows.

Green infrastructure (GI) is an approach to stormwater management that promotes natural processes of infiltration and evapotranspiration, reducing surface runoff to conventional stormwater drainage infrastructure [*Hamel et al.*, 2013]. In the urban context, GI functions by intercepting runoff close to where precipitation falls, and therefore is sometimes referred to as “source control” technology. Since the US EPA’s acceptance of GI and source control technologies for reducing combined sewer overflow events [*US EPA*, 2009], many cities with aging drainage infrastructure are seeking to incorporate GI design into their infrastructure plans as a cost-effective way of complying with federal and state regulations while also enhancing the livability of the urban environment .

Extensive monitoring has shown that GI is effective at the site scale in reducing peak flows and runoff volumes and enhancing water quality from precipitation events [*Davis*, 2007, 2008; *Emerson and Traver,* 2008; *Li et al.,* 2009; *Driscoll et al.,* 2015; *Page et al.,* 2015]. At the catchment scale, GI has also been shown to result in detectable differences in hydrological response [*Shuster and Rhea*, 2013; *Loperfido et al.*, 2014; *Bhaskar et al.*, 2016b; *Pennino et al.*, 2016]. Urban hydrological modeling studies have demonstrated the effectiveness of GI at the catchment scale [*Gilroy and McCuen*, 2009; *Ahiablame et al.*, 2013; *Burszta-Adamiak and Mrowiec*, 2013; *Lee et al.*, 2013; *Qin et al.*, 2013; *Palla and Gnecco*, 2015]. The effect of spatial distribution of GI at the catchment scale has been identified and explored using two-dimensional models [*Zellner et al.,* 2016]. However, most urban hydrological models of GI networks are lumped or semi-lumped parameter models that do not allow for the possibility of subsurface interactions or feedbacks that are distributed in space within the drainage area. This makes it difficult to distinguish between distinct hydrologic processes within the catchment, where there may be interactions between subsurface and surface processes [*Bhaskar et al.*, 2015].

Previous research suggests that such interactions or feedbacks may contribute significantly to the local water balance and hydrology in urban environments. The concept of Urban Variable Source Area (UVSA) is an adaptation of Dunne’s Variable Source Area (VSA), which states that heterogeneity of infiltration rates within a watershed has not only to do with the heterogeneity of soils; it is also dynamically related to the behavior of water over the topography of the landscape and in heterogeneous interactions with subsurface (shallow groundwater) capacity of soil [*Dunne et al.,* 1975]. UVSA extends idea to apply to urbanized areas, were high levels of spatial-temporal heterogeneity in topography, drainage infrastructure, buildings, human activities (such as lawn watering), and surface and subsurface conditions would be expected to dynamically affect the variable source area phenomenon [*Miles and Band*, 2015; *Lim*, 2016].

UVSA suggests that stormwater infiltration-based best management practices (BMPs) constructed at different locations within the catchment area could recover their storage capacities at different rates due to groundwater saturation, especially at topographic sag points [*Miles and Band*, 2015]. For example, studies have shown that (1) infiltration-based BMPs result in groundwater mounding, (2) mounding is more severe when BMPs are spatially clustered together, and (3) infiltration can exceed pre-development rates with widespread BMP adoption [*Gobel et al.*, 2004; *Endreny and Collins*, 2009; *Machusick*, 2009; *Maimone et al.*, 2011; *Bhaskar et al.*, 2016a]. The idea of "watershed capacitance" has been suggested as a way to characterize the degree to which runoff from impervious areas onto pervious areas can be stored, infiltrated or evapotranspired [*Miles and Band*, 2015]. Miles and Band [2015] defined "watershed capacitance" for watersheds retrofit with green stormwater infrastructure as: "the degree to which runoff from impervious surfaces directed to pervious surfaces can be infiltrated, stored and released slowly by baseflow or evapotranspiration."

The idea of watershed capacitance, which builds on Dunne's VSA theory of runoff generation, provides the theoretical foundation for a hypothesis on spatially differentiated effectiveness of infiltration opportunities in urban areas. Unlike groundwater storage, which typically refers to the volume of water held in the subsurface at some moment in time, watershed capacitance captures the potential of the watershed to mitigate runoff. It is spatially-dependent on the differential contraction of saturated areas within the watershed. A drainage area with "high capacitance" would not exhibit evidence of capacity limitations even under prolonged wet periods, multi-day events or large precipitation events. In other words, in an infinitely high capacitance watershed, if we could test multiple spatial configurations of infiltration opportunities, holding constant the total infiltration area, there would be zero capacity constraints and no negative feedback between saturated shallow groundwater and surface runoff. This would result in two possible outcomes in the differences in amounts of intercepted runoff. Either there would be no observable differences in performance between different spatial configurations, or spatial configurations located at "sag points," or areas of high accumulation, would be able to intercept more runoff than spatial configurations located in more spatially distributed upland areas. In both of these outcomes, locating infiltration opportunities in areas where capacity is likely to be more constrained due to inter-event capacity recovery does not have a negative effect on performance.

In contrast, drainage areas with "low capacitance" would exhibit signs of lowered effectiveness during prolonged wet conditions or large events, especially in patches of the drainage area that stay wet for longer periods, such as sag points in the topography. If we could test multiple spatial configurations of infiltration opportunities, holding the total receiving interception areas constant, we would expect capacity recovery to be slower in configurations where infiltration is placed in low-lying, high-accumulation areas of the watershed. Placement in areas of high accumulation would result in a negative effect on the capacity of the watershed to infiltrate or evapotranspire runoff onto receiving green infrastructure areas. Configurations where infiltration opportunities are located in upland areas would be expected to recover capacities more quickly between events.

In this research we explored watershed capacitance related to green infrastructure implementation. Using site data and observed runoff flows from an instrumented sewershed (an area that drains to a discrete point within a piped stormwater drainage system) that was retrofitted with green infrastructure BMPs between 2010 and 2015, we created a model domain to test how changes in porosity and hydraulic conductivity associated with green infrastructure result in differences in event-based the runoff ratios, accounting for potential negative feedbacks or lateral interactions due to capacitance limitations. While current studies have shown how GI can mitigate stormwater runoff, there are fewer studies that specifically explore to what extent the spatial configuration of GI networks influence the effectiveness of the entire network. In this study, changes in hydrologic regime and event-based runoff ratios for nine different scenarios were explored to determine how the idea of watershed capacitance relates to the spatial configuration of GI and impervious surfaces at the sewershed scale.

## 2 METHODS

In order to fully account for potential surface-subsurface vertical and lateral interactions hypothesized to result in VSA-type dynamics, we applied a fully-distributed, coupled surface-subsurface hydrological model, ParFlow.CLM to model the dynamics of an instrumented urban catchment. Our study consisted of three main steps. First, we used local and regional site data to parameterize and calibrate the model of the study site. Empirical flow data collected from a storm drain serving the sewershed before GI construction (2009 – 2010) and after GI construction (2015-2016) were used to calibrate the model and validate its capability to represent changes in the runoff response associated with GI installation. Second, we conducted scenario analyses on the calibrated model domain to evaluate the extent to which watershed capacitance is sensitive to the spatial configurations of changes in porosities and hydraulic conductivities associated with green infrastructure retrofits. We further developed the concept of watershed capacitance and its relation to event-based runoff ratios and the spatial configuration of green infrastructure using event-based runoff ratio metrics to characterize the study site's capacitance. Third, we used the level of variability observed in the monitored flow data as a benchmark against which to compare the variability in the scenarios' modeled event-based runoff ratios to evaluate the practical significance of differences in intercepted runoff volumes among spatial configuration scenarios. Each of these steps are described in further detail below.

## 2.1 Area Site Description

The study area is one of the sites of the "RiverSmart Washington" project, located in Washington D.C. Made possible through $4M in joint funding from the U.S. Fish and Wildlife Service, DC's Department of Energy and the Environment (DOEE), and DC Water, DOEE began the RiverSmart Washington monitoring program in 2009 to evaluate the effectiveness of GI retrofits to decrease runoff pipe flows at the catchment scale. The project began with in-pipe flow monitoring of the base case, pre-GI condition (PRE_GI), for six months as well as local precipitation monitoring in three sewersheds within the city [*DDOE et al.*, 2011]. This initial monitoring period was followed by extensive construction of GI within the study catchments and another post-GI construction six-month monitoring period. At the Lafayette site (**Figure 1**), which is the study site for this research (0.05 $km^2$, originally 34% impervious, with 15% building footprints and 19% pavement), the District Department of Transportation (DDOT) oversaw installation of bioretention bump-outs and permeable pavements designed to treat nearly all of the public right-of-way (ROW), and residents were offered subsidies to construct GI on their properties to treat runoff from their rooftops, driveways and private paths. In-pipe monitoring was conducted using an ADS Flowshark meter. The flow meter used four ultrasonic level sensors to record stage data, a low-profile Doppler velocity monitor, and a pressure sensor. The meter was linked to a cellular communications technology-enabled data logger. The Lafayette sewershed is served by a separate sewer system (stormwater runoff is conveyed by a separate system from domestic wastewater). Dry weather flow is limited to infiltration that occurs from seepage of groundwater into the pipes [*DDOE et al.*, 2011].

**Table 1** shows an inventory of the public right-of-way (ROW) retrofits total surface areas and contributing areas. Measurements were determined from construction documents provided to the authors by DOEE and dimensions of the constructed facilities were verified in the field.

**Table 1** Inventory of Public Right of Way BMPs implemented at the Lafayette site

| Description | Width (m) | Length (m) | BMP footprint ($m^2$) | BMP Contributing Area ($m^2$) |
|---|---|---|---|---|
| Permeable Pavement - ROW Gutter | 1.8 | 76.2 | 139.4 | 195.1 |
| Permeable Pavement - ROW Gutter | 1.8 | 70.4 | 128.8 | 149.4 |
| Permeable Pavement - Full width of alley | 4.3 | 48.5 | 207.1 | 0.0 |
| Bioswale - curb inlet extends off ROW | 2.7 | 12.8 | 33.9 | 105.8 |
| Permeable Pavement - ROW Gutter | 1.8 | 48.2 | 88.1 | 112.1 |
| Permeable Pavement - ROW Gutter | 1.8 | 87.6 | 160.1 | 227.1 |
| Bioswale in existing ROW | 1.4 | 29.6 | 41.5 | 168.1 |
| Permeable Rubber Sidewalk | 1.5 | 58.8 | 89.7 | 0.0 |
| Bioswale all outside ROW | 1.6 | 16.5 | 27.2 | 312.5 |
| Permeable Pavement - ROW Gutter | 1.8 | 74.2 | 135.7 | 152.0 |
| Permeable Pavement - ROW Gutter | 1.8 | 54.6 | 99.8 | 143.2 |
| Bioswale – curb inlet extends off ROW | 2.9 | 12.9 | 37.6 | 112.7 |
| Permeable Pavement - ROW Gutter | 1.8 | 28.7 | 52.5 | 73.2 |
| Permeable Pavement - Center of alley | 1.2 | 56.2 | 68.5 | 102.7 |
| Permeable Pavement - Center of alley | 1.2 | 70.1 | 85.5 | 128.2 |
| Permeable Pavement - ROW Gutter | 1.8 | 111.6 | 204.0 | 254.3 |
| Permeable Pavement - ROW Gutter | 1.8 | 111.6 | 204.0 | 292.1 |

| | | | | |
|---|---|---|---|---|
| Permeable Pavement - Center of alley | 1.2 | 104.6 | 127.6 | 350.8 |
| Permeable Pavement - Full width ROW | 9.3 | 41.9 | 389.9 | 0.0 |
| Bioswale all outside ROW | 1.4 | 13.7 | 19.5 | 66.1 |
| **Total** | | | **2340.2** | **2945.5** |

Of the 74 households within the sewershed, 25 agreed to install subsidized GI on their properties, resulting in the disconnection of over 1,400 m$^2$ of residential rooftop and over 550 m$^2$ of private paths and driveways. Before GI construction, residential downspouts were all physically connected to the storm drain system by a buried PVC pipe that drained either directly into the street or the adjacent sidewalk.

Residents choosing to participate in the RiverSmart Washington retrofit program were offered a selection of potential BMPs that included: permeable pavers, rain gardens, bayscaping (native landscaping), and rain barrels. **Table 2** shows an inventory of residential retrofits and site summary statistics. Retrofits are grouped based on vegetated and non-vegetated BMPs: bayscaping and rain gardens are vegetated BMPs that intercept runoff from roofs and other impervious surfaces and increase the permeability of native soils through amending soils; permeable pavements are non-vegetated BMPS that increase permeability of impervious surfaces and provide storage in an underlying gravel bed layer.

**TABLE 2.** Inventory of Private GI Retrofits at the Lafayette site

| **Site Component** | **Area (m$^2$)** |
|---|---|
| Sewershed Total Area | 52,000 |
| 2010 Total Impervious Area | 22,000 (42%) |
| Total Private Property Area | 37,000 (71%) |
| Lot size | |
| Min | 5 |
| Max | 1,490 |

| | |
|---|---|
| Median | 528 |
| Mean | 499 |
| Disconnected Roofs (draining to rain barrels, rain gardens, permeable pavement, or lawn) | 1,423 |
| Treated Pavement (permeable pavement) | 552 |
| Amended Lawns (rain gardens) | 195 |

**Figure 1** depicts the boundary of the Lafayette sewershed with locations of public and private GI installations and the monitoring location.

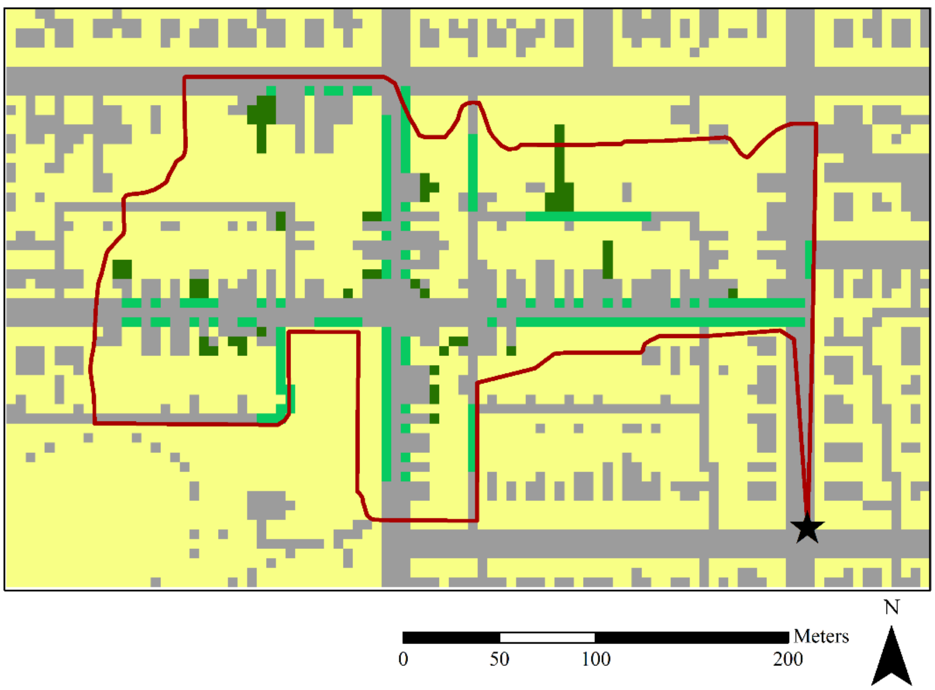


**Figure 1.** Domain of the Lafayette sewershed with locations of implemented public and private installations of GI and monitoring point. Yellow: untreated pervious; Gray: impervious; Light green: pavement-type green infrastructure (located in public ROW). Dark green: vegetation-type green infrastructure (located on private properties). Red outline: area draining to sewer outlet (sewershed boundary). Star: outlet monitoring location (in a storm pipe).

## 2.2 Model Description and Parameter Inputs

All simulations were carried out with ParFlow.CLM. ParFlow is an integrated physical hydrology model that couples both surface and subsurface flow through continuous, finite-difference solutions to Richards equation [*Ashby and Falgout*, 1996; *Kollet and Maxwell*, 2008; *Maxwell et al.*, 2016]. Surface flow is simulated via the kinematic wave equation whenever the pressure in the top cells of the domain are greater than zero. To simulate water-energy fluxes between the land surface and atmosphere, ParFlow has been coupled to the land surface model CLM, allowing for representation of evapotranspiration [*Oleson*, 2010; *Condon and Maxwell*, 2014]. In this application, we opted to use the terrain-following-grid and variable dz options of ParFlow [*Maxwell*, 2013].

The subsurface domain was defined with 12 layers of variable thickness for the terrain-following grid extended to a total depth of 50 m below the land surface. Including this depth in the model with the chosen boundary conditions increased the stability of the underlying water table and prevented positive pressure buildup in low-lying areas of the site. The thicknesses for the twelve layers from topsoil/pavement to bedrock were: 0.05 m, 0.05 m, 0.05 m, 0.5 m, 0.5 m, 0.5 m, 0.75 m, 2.5 m, 5 m, 5 m, 10 m and 25.1 m. The horizontal resolution chosen for the domain was 5 m x 5 m. The model was run at a 0.1 h time step.

We made two major modifications to the original site data in order to represent the overland flow routing behavior of the conventional drainage infrastructure and GI retrofits. First, to reflect the true routing of roofs to the storm drain system, we moved the building footprints to be adjacent to the street. This better represented the base-case scenario (PRE_GI) of rooftops immediately gaining hydraulic connectivity to the storm drain system without having to create subgrade flow paths to represent the small buried pipes that connected roofs to the storm drain system in reality. Second, the main drainage system pipe was represented by "burning in" the centerline of the ROW, to enforce drainage of the site towards the drainage infrastructure. After DEM modifications, a global slope enforcement algorithm was applied to ensure good drainage of the domain [*Barnes et al.*, 2015]. The storm drain system is not pressurized and does not experience surcharging during precipitation events, therefore these simplifications treat the pipe as open channel flow.

**2.2.1 Local Geologic Parameters**

As part of the extensive DDOT GI construction, geotechnical analyses of 32 boring locations distributed throughout the site provided much detail on the hydraulic conductivity conditions of the site to 2-m depth [*HSA, Inc*, 2012]. Geotechnical reports included sieve analyses from two depths for each boring: between 1.2 m – 1.8 m, and between 1.8 m – 2.4 m. From the sieve analyses' particle distributions, we calculated the mean tenth percentile passing ($d_{10}$) across the 32 borings at each of the two sample depths. The geotechnical reports include depths of defined strata (topsoil, asphalt, concrete, estimated fill, and native soil) for each boring, soil descriptions (sand, silt, clay composition), and results for two sieve analyses for each boring location. Hydraulic conductivity for depths between native soils and backfill up to the depth of 2.44 m were calculated from the HSA sieve analysis using the Hazen formula [*Vienken and Dietrich*, 2011].

The geotechnical reports indicated pavement thicknesses ranging from 0.2 m – 0.3 m. The geotechnical reports focused on conditions within the public ROW and in alleys, since this is where the design of public BMPs were located. However, a few borings were located in the turf strip between the ROW and the sidewalk. These borings indicated that in pervious areas, the average topsoil thickness was 5 cm.

Paved ROWs and alleys either have asphalt or concrete surfaces. In asphalt-covered ROWs/alleys, underlying 7.6 cm of asphalt is approximately 23 cm of fill. Concrete used in alleys is 23 cm thick. Since site geotechnical reports stated that the fill is compositionally and visually similar to the surrounding native soil, we assumed fill properties were similar to the shallower of the two soil analyses performed at each boring location. The first 15 cm of the subsurface domain in ROWs and alleys was therefore defined as pavement. The properties of underlying fill layers were assigned the hydraulic properties of native soils as determined by the sieve analyses.

Topsoil was assigned a saturated hydraulic conductivity $K_s = 3.75 \times 10^{-4}$cm/s and porosity 0.4, based on the mean of field-measured values in an urban environment in nearby urban Virginia [*Chen et al.*, 2014]. Impervious pavement (both asphalt and concrete) were assigned $K_s = 8.5 \times 10^{-7}$ cm/s and porosity of 0.1% based on values reported in the literature for measured hydraulic properties of asphalt (Kuang et al., 2011).

The chosen horizontal grid resolution of the model (5 m x 5 m) is larger than many of the footprints of the private GI installations. Therefore GI grid cells represented the weighted average of hydraulic properties of both the BMP retrofit and its contributing area, according to the relative areas of each. The properties assigned for pavement-based GI and vegetated based GI are presented in **Table 3.** The hydraulic conductivities used for the weighted calculations were derived primarily from DDOT's construction specifications for backfill materials and the Hazen equation. Where specifications were not available, typical values from industry and academic literature were used. Areas that were retrofit with GI consisted of the footprint of the GI BMP facility itself, as well as the contributing area that was designed to contribute stormwater runoff onto the BMP. In the model, the designed contributing area and the GI facility footprint were represented together over their combined footprint. The hydrologic parameters for the combined footprint (porosity and hydraulic conductivity) were represented as a weighted average of the parameters of each based on their original footprints.

### 2.2.2 Regional Geologic Properties

As is shown in **Figure 2**, the geology of Washington DC spans the Piedmont and Atlantic Coastal Plain physiographic regions; the zone where these two physiographic provinces intersect is designated as the Fall Line or Fall Zone. The Lafayette site is located in the Piedmont physiographic region [*HSA*, *Inc*, 2012].

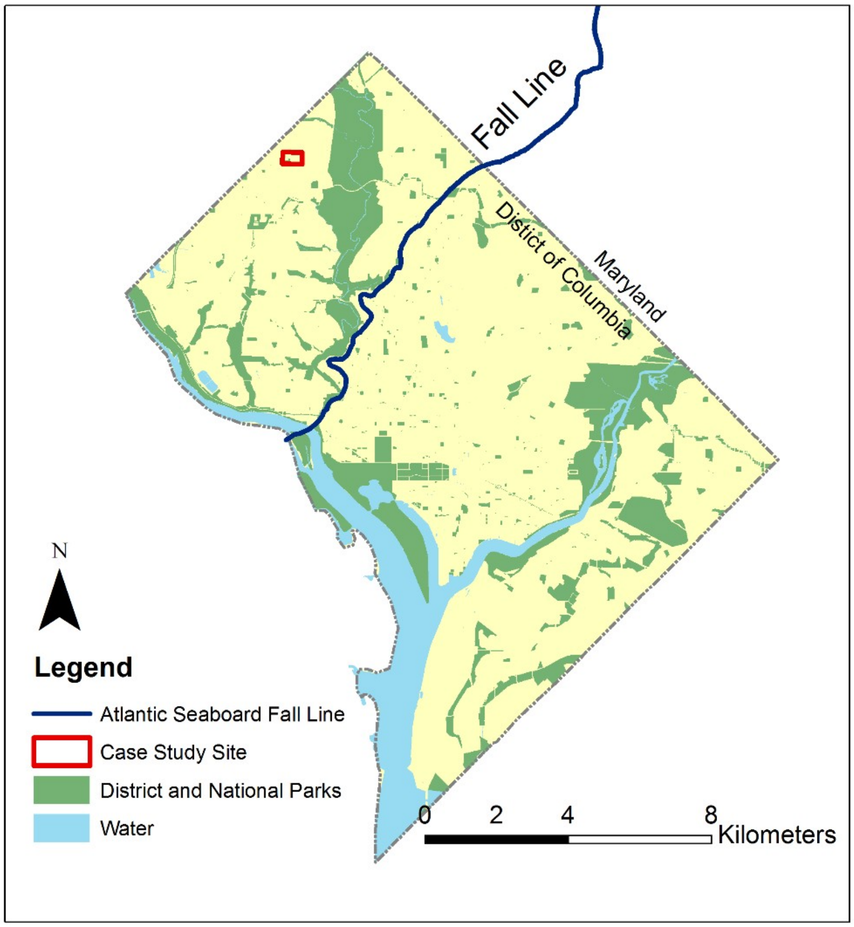


**Figure 2.** Location map showing site location within the District of Columbia

Beyond the 2.35 m of site-specific geotechnical reports defining the soils properties of the site, deeper soil hydraulic properties were defined from regional data. . The Piedmont physiographic province is defined by layers that include soil, saprolite, a transition zone of high-hydraulic conductivity, highly-weathered fractured rock, and fractured bedrock. We defined geologic layer thicknesses based on regional geological survey reports. Thicknesses of the layers, geologic properties and sources of information are summarized in **Table 3**.

### 2.2.3 Vegetative and Impervious Cover

A high-resolution vegetative cover dataset of the DC metro area was provided by researchers at the University of Vermont [*University of Vermont*, 2011]. This dataset had 1-m resolution and included six land cover/vegetation classifications within the Washington DC area: bare soil, buildings, roads/railways, other paved surfaces, grass, tree canopy, and water. The CLM portion of the model, which controls meteorological forcing, energy fluxes, and evapotranspiration, requires that all grid cells be assigned a vegetative cover classification [*Maxwell et al.*, 2016]. The UVM land cover dataset was reclassified to three types of vegetative cover: tree canopy, urban and built, and grassland. These land covers were selected to represent the differences in tree canopy interception and fallthrough and evapotranspiration processes associated with different types of vegetation. In our simulations, we used the default parameters for the CLM portion of the model for each of these vegetative cover classes [*Maxwell et al.*, 2016].

The impervious/pervious land cover classification used for both for defining the CLM vegetative cover and for the assigning hydraulic properties were rasterized from vector polygons of building footprints, and ROW boundaries from DC’s Office of the Chief Technology Officer (OCTO).

**TABLE 3 – Hydraulic Properties Assigned To Domain Subsurface Based on Land Cover Type**

**Land-Cover Specific Subsurface Layers**

| Layer | Thickness (m) | Depth to Bottom (m) | Description | Ksat (cm/s) | Porosity | Ksat Source/Method | Porosity Source/ Method |
|---|---|---|---|---|---|---|---|
| **Pervious** | | | | | | | |
| 1 | 0.05 | 0.05 | Topsoil | 3.75E-04 | 0.460 | Chen *et al.* 2014 midpoint of reported range | Porosity curve from Cunningham and Daniel (2001) |
| 2 | 0.05 | 0.1 | Soil 1 | 8.14E-06 | 0.400 | HSA Geotechnical Report; Hazen formula | |
| 3 | 0.05 | 0.15 | Soil 1 | 8.14E-06 | 0.400 | | |
| 4 | 0.5 | 0.65 | Soil 1 | 8.14E-06 | | | |
| **Impervious - ROW, Roofs** | | | | | | | |
| 1 | 0.05 | 0.05 | Impervious | 8.50E-07 | 0.001 | Kuang *et al.* 2011; lower end of reported range | Skellyand Loy, 2011; reported value |
| 2 | 0.05 | 0.1 | Impervious | 8.50E-07 | 0.001 | | |
| 3 | 0.05 | 0.15 | Impervious | 8.50E-07 | 0.001 | | |
| 4 | 0.5 | 0.65 | Soil 1 | 8.14E-06 | 0.450 | HSA Geotechnical Report; Hazen formula | Porosity curve from Cunningham and Daniel (2001) |
| **GI - vegetated** | | | | | | | |
| 1 | 0.05 | 0.05 | Bioinfiltration Media | 3.25E-03 | 0.043 | Construction document specifications; Hazen formula | DDOT specification, AASHTO standard |
| 2 | 0.05 | 0.1 | Bioinfiltration Media | 3.25E-03 | 0.043 | | |
| 3 | 0.05 | 0.15 | Storage | 2.04E+00 | 0.068 | | |

| | | | | | | | |
|---|---|---|---|---|---|---|---|
| 4 | 0.5 | 0.65 | Storage | 2.04E+00 | 0.068 | | |
| **GI - pavement** | | | | | | | |
| 1 | 0.05 | 0.05 | Permeable Pavement | 3.30E-05 | 0.010 | Construction document specifications; Hazen formula | DDOT specification, AASHTO standard |
| 2 | 0.05 | 0.1 | Permeable Pavement | 3.30E-05 | 0.010 | | |
| 3 | 0.05 | 0.15 | Storage | 2.04E+00 | 0.068 | | |
| 4 | 0.5 | 0.65 | Storage | 2.04E+00 | 0.068 | | |
| **Common Subsurface Layers** | | | | | | | |
| 5 | 0.5 | 1.15 | Soil 1 | 8.14E-06 | 0.450 | HSA Geotechnical Report; Hazen formula | Porosity curve from Cunningham and Daniel (2001) |
| 6 | 0.5 | 1.65 | Soil 2 | 5.42E-06 | 0.470 | | |
| 7 | 0.75 | 2.4 | Soil 2 | 5.42E-06 | 0.470 | | |
| 8 | 2.5 | 4.9 | Saprolite | 1.43E-03 | 0.470 | Nutter and Otton, 1969; mean of reported | |
| 9 | 5 | 9.9 | Saprolite | 1.78E-03 | 0.470 | Nutter and Otton, 1969; Green *et al.* 2004; mean of reported | |
| 10 | 5 | 14.9 | Transition Zone | 3.58E-03 | 0.470 | Nutter and Otton, 1969; Mace 1997; mean of reported transmissibility, divided by depth of regolith | |
| 11 | 10 | 24.9 | Bedrock | 1.26E-04 | 0.050 | Paulachok 1991, Low *et al.*, 2004; Andino (2015) well yields method | |
| 12 | 25.1 | 50 | Bedrock | 8.25E-05 | 0.020 | | |

### 2.2.4 Meteorological Data

We assembled meteorological data by combining site-specific precipitation monitoring from the RiverSmart Washington Program and National Land Data Assimilation Systems (NLDAS) meteorological forcing data [*Mitchell*, 2004], which includes hourly records for air pressure, temperature, wind speed, humidity and solar radiation retrieved for the site based on geographic coordinate-specified boundaries.

### 2.2.5 Boundary Conditions, Model Spinup, and Calibration

A 20-m difference in pressure head between the eastern and western faces was set to represent the approximately constant empirical depth to groundwater in the Piedmont areas of the District of Columbia. Zero flux boundary conditions were set on the northern, southern, and bottom faces of the domain box. An overland flow boundary condition and meteorological forcing conditions (precipitation, evapotranspiration) coupled through the CLM portion of the model were used for the top of the domain. Spinup was carried out in two stages, as has been described by others, in order to reach dynamic equilibrium before scenario testing [*Ajami et al.*, 2014; *Seck et al.*, 2015].

The observed before-and-after GI in-pipe flow data was used to calibrate and validate the model. First, the pre-GI parameterization (PRE_GI, shown in **Figure 2**), was used to calibrate the model. Because of the computational expense of running full simulation runs of ParFlow, several characteristic precipitation events from the before period were selected to calibrate Manning's n. Manning's n was the only parameter selected for calibration to avoid issues of equifinality. **Figure 3a** shows a comparison between the simulated channel flow from the domain (computed at the monitoring location) and the observed flows measured at the monitoring location for one of these events (August 5th, 2010) for PRE_GI (**Figure 2**). The calibration procedure is explained in Bhaskar *et al*. (2015). Despite the slight delay of the simulated flow peak (shown in **Figure 3a**) compared to the observed flow peak, we accepted the calibration as adequate because the meteorological forcing input to the CLM portion of ParFlow.CLM smooths out peak rain intensities that would have resulted in faster overland flow response from the site.

After calibration, a further comparison was made using the monitored and simulated flows for the post-GI construction configurations (POST_GI) and parameterization for several characteristic events. The POST_GI configuration reflected the actual locations of GI retrofits of the site (total treated areas shown in **Table 1** and **Table 2)**. One comparison between the observed and simulated event hydrographs (July 1st, 2015) is shown in **Figure 3b**. Compared to the observed flows measured at the monitoring site, the simulated peak is both delayed and smaller in magnitude. Although not a precise match, we accepted the calibrated Manning's n for the modeled domain's capability to adequately represent the changes in the parameters of the domain associated with the GI retrofits for three reasons. First, the muted simulated peak compared to the empirical peak is partially explained by the limitations in input for precipitation (hourly NLDAS data) which does not capture peak precipitation intensities in the monitoring data. Second, further adjustments of Manning's n did not improve the timing match between empirical and simulated hydrograph peaks. Third, because of the resolution of the model (5 m x 5 m), more impervious surface area in the modeled base case is treated with GI than was actually treated in reality (see **Table 4** for a comparison of empirical and modeled land cover classifications). We therefore used this Manning's n for the remaining simulations.

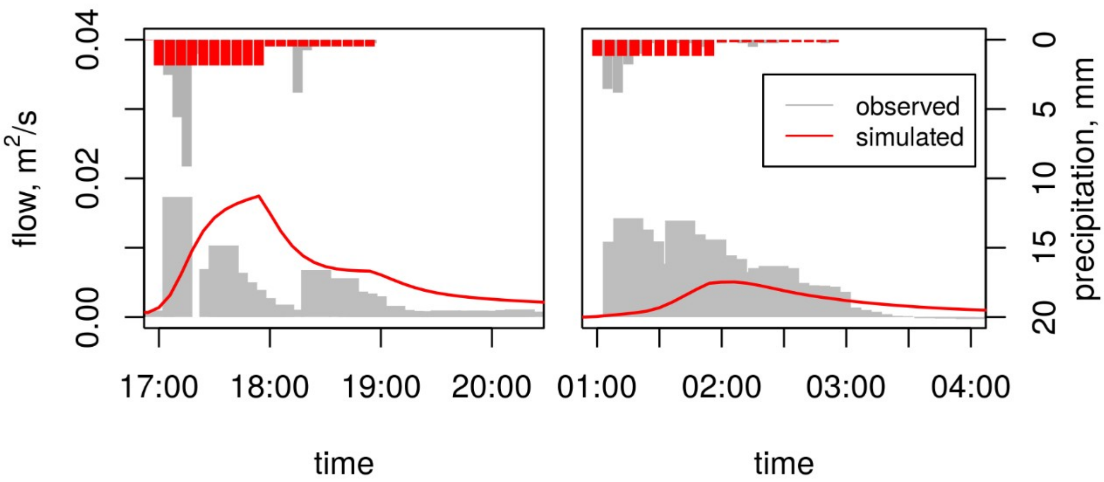


**Figure 3 a**) Comparison of hydrographs for a precipitation event (August 5$^{th}$, 2010) used for calibration of Manning's n in the pre-GI construction configuration and parameterization of the study site domain. **b)** Comparison of hydrographs for a precipitation event (July 1$^{st}$, 2015) used to evaluate performance of the calibrated parameters for the post-GI construction configuration (POST_GI) and parameterization of the study site domain.

Flow duration curve comparisons were also made between the simulated flows and the empirical monitored flows from the site in order to evaluate the model's representation of the site hydrology (**Figure 4**). Several high-level trends are apparent in **Figure 4**. First, all scenarios exhibit larger simulated baseflows than what is observed from the monitoring data. This includes the simulated Base, which had equal levels of imperviousness with connected roofs as the empirical Base, and the simulated IS_DISC and IS_MAX, which had equal, and higher levels of imperviousness with disconnected roofs, respectively. Both the empirical Base and empirical GI flows do not exhibit many baseflows. This pattern could be due to either lack of sensor sensitivity to low (dry weather) flows or an actual lack of baseflows within the pipe during nonrain events and the model's overestimation of baseflows. Although simulated low flows are larger than empirical flows, Figure 4 shows relatively good agreement between the top 15% of flows between the simulated and empirical data. The FDCs show the distribution in peak flows to be underestimated by the model. However, this comparison does not control for all possible confounding effects, since the rainfall total depth and intensity profiles for the empirical data and the simulation period also differ.

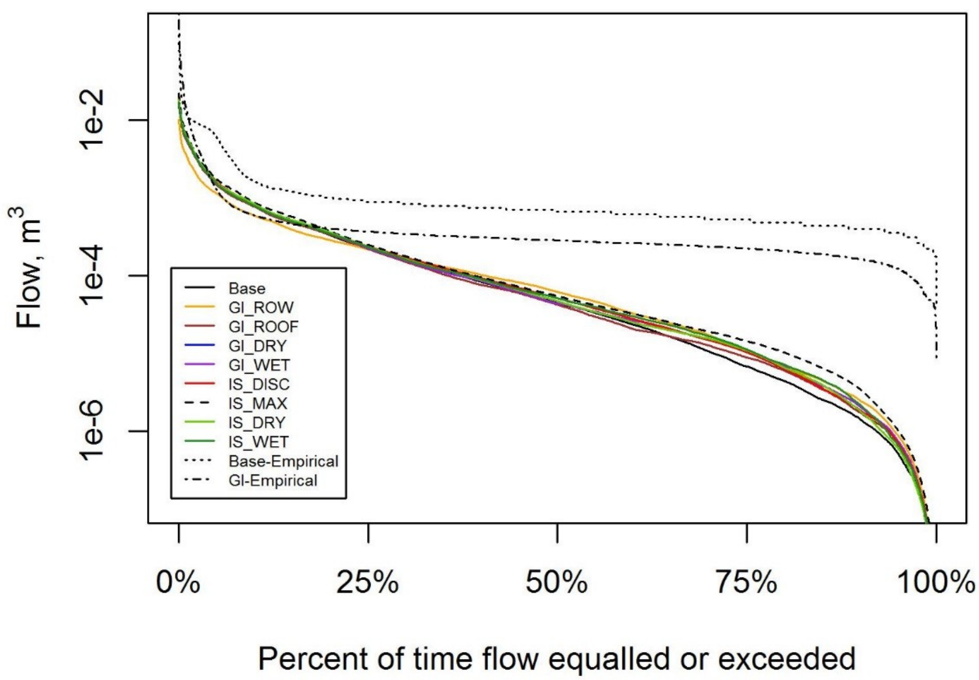


**Figure 4** Flow Duration Curves of simulated scenarios and empirical observed pipe flows

### 2.2.6 Computing Resources

ParFlow is optimized to run on parallel computing resources. The simulations in this study were run on 256 processors (16 nodes) on the "Stampede" computing cluster at the Texas Advanced

Computing Center, accessed through the NSF Extreme Science and Engineering Discovery Environment (XSEDE) platform. The model domain had a total of 69,120 cells distributed with 16 process splits in the x direction, 16 process splits in the y direction, and 1 process split in the z direction. Each scenario's production run simulation of the six month period (described below) necessitated between 35 h to 42 h of wall-clock time.

## 2.3 Scenarios

After spinup and calibration, nine scenarios were tested to determine how spatial configurations of green infrastructure and impervious surfaces affect local hydrology. Each scenario was simulated using a six-month period of meteorological forcing data (March 1, 2015 – September 1, 2015). This period was chosen as a representative year because the total annual precipitation depth in 2015 (1107.4 mm) was the precipitation depth closest to the mean total annual precipitation from the 1949-2015 (1127.3 mm).

All scenarios were run with the same CLM settings, site topography, and tree canopy inputs. All scenarios were initialized with the pressure field output from the equilibrated spinup. For each scenario, the pervious- and impervious-assigned Manning's n, porosity and permeability were distributed according the spatial configuration conditions of the scenario. Scenarios were developed to meet the dual goals of practical implementation and to capture and control for physical variation of the site, in order to best identify specific physical processes causing differences in model output.

We considered three major practice-relevant decisions regarding the spatial configuration of GI networks at the sewershed scale. First, how construction of GI in the public ROW, where flow accumulation is highest, compares to treating the same magnitude of impervious surface area on private properties, where the latter is likely to result in cost savings but require much more coordination and outreach to private property owners. Second, how targeting different properties for treatment within the sewershed, based on the average wetness of the property, could impact efficacy of the overall GI network. Lastly, we also considered two sewershed-wide property-scale changes: roof downspout disconnection of all properties and maximum allowable impervious surface area on all properties. Complete descriptions of all scenarios tested are given in the following sections and are summarized in **Table 4**.

### 2.3.1 GI Configuration Scenarios

#### 2.3.1.1 GI_ROW: Treat ROW

In this scenario (**Figure 5**), all of the areas in the public ROW were treated with green infrastructure with properties specified by the pavement-type construction specifications described in Section 2.2.1. Because GI that treats the ROW treats flows from the surface and does not intercept flows from the subgrade pipe, the pipe, burned in at the centerline of the ROW is assigned properties of "untreated" impervious surface (Manning's roughness coefficient, hydraulic conductivity, and porosity). This scenario is paired with GI_ROOF, which treats an approximately equal amount of roof area, located on distributed private properties. The practical implementation implication of these two scenarios informs to what extent differences in hydrologic efficacy can be expected to drive decisions between public investment in GI in the ROW, which is more costly, compared to investment in subsidies for private property owners to retrofit their own properties, which has the potential to result in large cost savings for urban stormwater infrastructure managers [*Valderrama and Levine*, 2013].

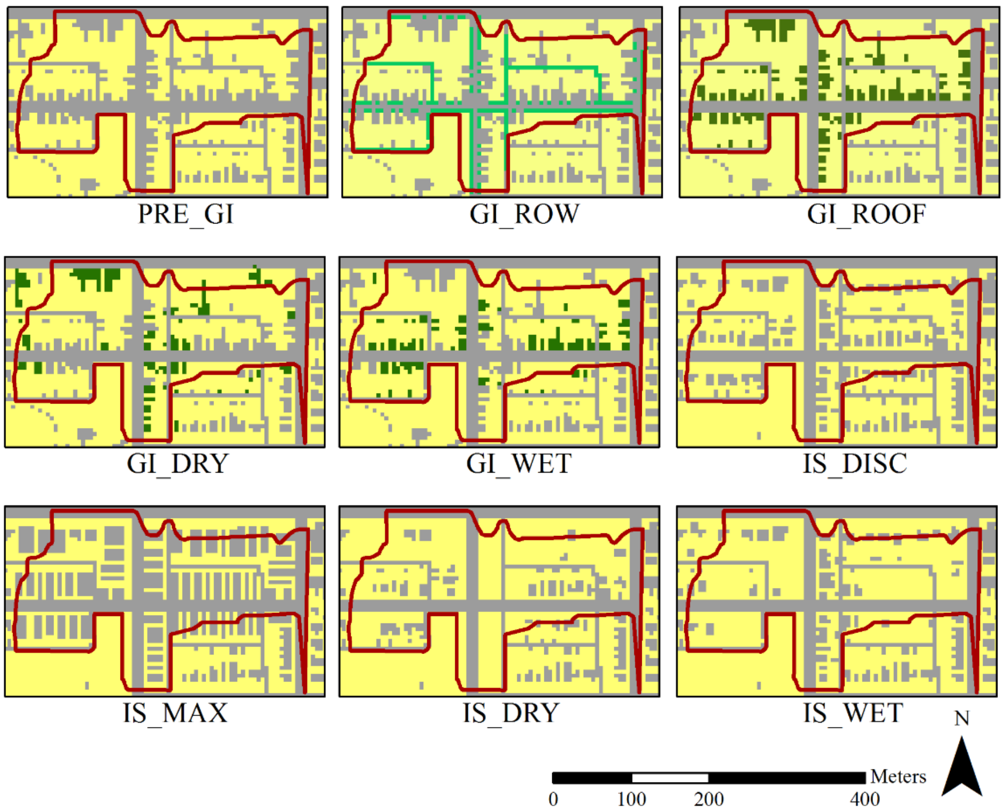


**Figure 5.** Scenario land covers used to assign hydraulic conductivity, porosity, and values of Manning's roughness coefficient. Yellow: pervious; Gray: impervious; Light green: pavement-type green infrastructure. Dark green: vegetation-type green infrastructure. Red outline: sewershed boundary. From top to bottom, left to right: PRE_GI, GI_ROW, GI_ROOF, GI_DRY, GI_WET, IS_DISC, IS_MAX, IS_DRY, IS_WET, as defined in **Table 4**.

#### 2.3.1.2 GI_ROOF: Treat Roofs

An area equal to the total treated ROW in scenario GI_ROW is treated at the building footprints in scenario GI_ROOF. Compared to GI_ROW retrofits, which correspond at the areas of highest flow accumulation in the sewershed, GI_ROOF retrofits are spread over higher elevations, and have lower average flow accumulation. The parameters used for the roof retrofits were those specified by the vegetation-type construction specifications described in **Section 2.2.1.**.

#### 2.3.1.3 GI_DRY and GI_WET: Treat Roofs of Low/High Accumulation Properties

In addition to testing differences between GI located in the ROW versus on roofs, we tested two spatial scenarios that treated roofs located on properties with the highest versus lowest average flow accumulation values of the sewershed. These scenarios were meant to explore if location of GI on "wetter" (higher average flow accumulation) properties would show signs of lowered capacitance, and, whether specific properties within a sewershed should be targeted to optimize efficacy of the GI network. In these scenarios, properties with the lowest/highest mean flow accumulation values (averaged over flow accumulation values for the entire property area) were selected to treat with the vegetation-type GI respectively for GI_DRY and GI_WET. Because properties varied in roof area, there was not perfect control of area removed between the two scenarios. GI_DRY treated 4,930 $m^2$ of impervious surface from the domain, while GI_WET treated 4,318 $m^2$ of impervious surface.

### 2.3.2 Impervious Surface Configuration Scenarios

#### 2.3.2.1 IS_DISC: Disconnect Roofs

The IS_DISC scenario is identical to the PRE-GI scenario for the site, except that the building footprints were not moved to be adjacent to the ROW. Relocating building footprints adjacent to the ROW in the PRE_GI scenario represented the direct routing of roof runoff to the storm drain collection system. The IS_DISC scenario therefore tested the relative impact of simply disconnecting roof downspouts and routing them onto lawns, with no additional amendments to the porosity and storage capacity in the soils (as was done in the GI scenarios).

**2.3.2.2 IS_MAX: Allow Maximum Impervious Surface Area per Property**

To construct the IS_MAX scenario the highest allowable impervious area coverages per zoning code was assigned to each parcel within the sewershed. This scenario represents a future, maximum level of imperviousness on the site that could potentially occur if all owners maximized lot coverages.

**2.3.2.3 IS_DRY and IS_WET: Remove Impervious Surface areas on Low/High Flow Accumulation Properties**

The IS_DRY and IS_WET scenarios tested the impacts of siting impervious surface area relative to topography-determined high and low flow accumulation paths within a drainage area. In the same way used for the GI_DRY and GI_WET scenarios, properties with the lowest (IS_DRY) and highest (IS_WET) mean flow accumulation values per property were chosen for impervious surface area removal. Comparison of the results of these scenarios is relevant for site planning to minimize runoff peaks, or in the case of shrinking or heavily vacant areas, targeted removal of imperviousness to increase the efficiency of infrastructure remaining on the site. Assigned hydraulic conductivities of treated roofs are lower (top layer $K_{sat}$ = 0.000375 cm/s) and porosities are higher (top layer porosity = 0.46) for IS_DRY/IS_WET than for GI_DRY/GI_WET (top layer $K_{sat}$ = 0.00325 cm/s, top layer porosity = 0.043).

**Table 4** Scenario Summaries

| **Scenario** | **Impervious ($m^2$)** | **Pervious, non-GI ($m^2$)** | **Vegetated GI ($m^2$)** | **Pavement GI ($m^2$)** | **Percent Impervious** | **Percent Impervious Treated** |
|---|---|---|---|---|---|---|
| PRE_GI-empirical | 22000 | 30000 | 0 | 0 | 42 | 0 |
| POST_GI-empirical | 18025 | 29805 | 195 | 1925 | 35 | |
| PRE_GI | 23375 | 29450 | 0 | 0 | 44 | 0 |
| POST_GI | 17350 | 29450 | 1600 | 4200 | 33 | 26 |
| GI_ROW | 15875 | 29450 | 0 | 7500 | 30 | 14 |
| GI_ROOF | 15150 | 29450 | 8225 | 0 | 29 | 16 |
| GI_DRY | 19500 | 29450 | 3875 | 0 | 37 | 7 |
| GI_WET | 19025 | 29450 | 4350 | 0 | 36 | 9 |
| IS_DISC | 23850 | 28975 | 0 | 0 | 45 | 0 |
| IS_MAX | 31900 | 20925 | 0 | 0 | 60 | 0 |
| IS_DRY | 19325 | 33500 | 0 | 0 | 37 | 7 |
| IS_WET | 20100 | 32725 | 0 | 0 | 38 | 9 |

| **Scenario** | **Description** | **Colors** |
|---|---|---|
| PRE_GI | No treatment with GI; All roofs connected via downspout | Gray/black |
| GI_ROW | All impervious area in ROW treated with permeable pavement GI; roofs connected | Orange |
| GI_ROOF | Equal roof area as GI_ROW treated with vegetative GI | Brown |
| GI_DRY | Roofs located on low flow accumulation properties treated with GI | Blue |
| GI_WET | Roofs located on high flow accumulation properties treated with GI | Purple |
| IS_DISC | All roofs disconnected from storm drain in ROW | Red |
| IS_MAX | Maximum imperviousness on every property | Black-dashed |
| IS_DRY | Roofs located on low flow accumulation properties replaced with native soil | Light Green |
| IS_WET | Roofs located on high flow accumulation properties replaced with native soil | Dark Green |

## 2.4 Evaluating Sewershed Capacitance

We used two methods to evaluate sewershed capacitance of the site. First, flow duration curves (FDCs) were used to compare the overall distributions of overland flow patterns ranging from storm peak flows to baseflows for each scenario. The lower the sewershed capacitance of a site, the more significant the effects of differential saturation contraction, and the more of a difference we would expect to see between FDCs of different spatial configuration scenarios. Second, we developed a measure of scenarios' event-based 'efficiencies' compared to the PRE_GI case. FDCs allow for comparisons of entire distributions of flows, while event-based analysis allows for an examination of a subset of runoff behaviors.

A script was written in R to isolate the peaks and total precipitation volumes associated with each precipitation event from the simulated overland flow and monitored pre- and post-GI time series Runoff behaviors can vary depending on the size and intensity of the precipitation event, as well as the pre-event wetness or inter-event period. According to theory, a watershed that is highly sensitive to pre-event wetness would be expected to infiltrate less runoff when inter-event periods are short (and the watershed has less time to recover storage capacity) than a watershed that is less sensitive to pre-event wetness. Similarly, if a watershed is capacity-limited, then we would expect GI in low-lying, high flow accumulation locations in the watershed to perform less effectively than GI in upland areas which would be expected to recover capacity more quickly. If, on the other hand, a watershed has high capacitance [*Miles and Band*, 2015], then perhaps GI in low-lying, high-flow-accumulation locations in the watershed would perform more effectively than GI in upland areas, since in addition to their direct contributing areas, they would intercept other upland areas' flows.

Precipitation events were identified based on inter-event dry periods of at least 10 hours. If precipitation stopped, but started again in less than 10 hours, both periods were counted as part of the same precipitation 'event.' All runoff values (as calculated at the pour point) between the onset of flows and when flows returned to zero were summed to define a total event volume of runoff.

Total volumes mitigated by GI retrofits and impervious surface removed were calculated by subtracting the total event-based runoff volumes from each of the alternative scenarios from the total event-based runoff volumes from the PRE_GI case. In addition, since the paired spatial configuration scenarios included slightly different totals of impervious surface retrofit, per-m$^2$ volumes intercepted for each event were calculated based on the total treated/removed area of impervious surface for the scenario. This was a way of assessing per-m$^2$ efficacy of the GI retrofits. **Equation 1** summarizes the calculation:

$$E_{S_{i,j}} = \frac{\int_i^j \left(Q_{Base} - Q_S\right) dt}{A_S} \qquad [1]$$

where $E_{S_{i,j}}$ is the area-normalized efficacy [L] of scenario $S$ for the event defined by $(i,j)$; $Q_{Base}$ is the flow rate for the PRE_GI case scenario [L$^3$T$^{-1}$]; $Q_S$ is the flow rate for scenario $S$; $A_S$ is the total area of [L$^2$] treated/removed impervious surface in scenario $S$; $(i,j) \in \{(i_1, j_1), (i_2, j_2) \ldots (i_n, j_n)\}$ are paired times marking the start and end of events $1 \ldots n$ for $n$ is total number of precipitation events; and $S \in \{GI2A, GI2B, GI3A, GI3B, IMP3A, IMP3B\}$ is a paired spatial configuration scenario. The area-normalized efficacy $E_{S_{i,j}}$ for each defined event can also be understood as the average mitigated depth of precipitation per square meter of GI.

$E_{S_{i,j}}$ was also conditioned on the depth of the precipitation events to explore how effectiveness of each spatial configuration compared to PRE_GI changed under wetter conditions. This conditioning was done through the linear regression of $E_{S_{i,j}}$ on event precipitation depth. A steeper estimated slope of the coefficient from linear regression would indicate that the treatment/removal of imperviousness intercepts more runoff compared to the PRE_GI scenario (i.e., it is more effective).

There was a particular interest in explaining the circumstances under which the high flow accumulation configuration has a greater E value than the low flow accumulation configuration, and vice versa. For example, out of 72 identified precipitation events, $E_{GI2A} > E_{GI2B}$ for 48 events, while $E_{GI2B} > E_{GI2A}$ for 24 events; out of 72 identified precipitation events $E_{GI3B} > E_{GI3A}$ for 32 events, while $E_{GI2B} > E_{GI2A}$ for 40 events; and out of 45 identified precipitation events, $E_{IMP3B} > E_{IMP3A}$ for 12 events.

In order to more closely examine if there was statistical evidence that either total event precipitation depth or the inter-event period influenced whether the high flow accumulation or low flow accumulation spatial configuration was more effective in reducing the precipitation-runoff ratio, an additional analysis was performed. Events where the spatial configuration treating or removing imperviousness on low flow accumulation (DRY) properties performed better (higher E) than the spatial configuration treating or removing imperviousness on high flow accumulation (WET) properties were defined as the function *g* **(Equation 2)***:*

$$g\left(x_{i,j}\right)\begin{cases}0\ x_{i,j}\in\left\{E_{DRY,i,j}>E_{WET,i,j}\right\}\\1\ x_{i,j}\in\left\{E_{WET,i,j}>E_{DRY,i,j}\right\}\end{cases} \qquad [2]$$

where $x_{i,j}$ is the precipitation event defined by start time *i* and end time *j*; $E_{\{DRY,WET\},i,j}$ are the E values calculated in **Equation 1;** and DRY scenarios include GI_ROOF, GI_DRY, and IS_DRY and WET scenarios include GI_ROW, GI_WET, and IS_WET. We then tested the dependence of the $g\left(x_{i,j}\right)$ binary state classification on total precipitation depth and inter-event period. If the state classification is independent of these conditions then the state assignment should be random with respect to the condition. If on the other hand, the state classification is shown to be dependent on these conditions, then a comparison of the condition means between the two states can reveal a causal explanation for higher or lower efficacy *E* of the intervention.

The statistical significance of the dependence of the binary state classification on total event precipitation depth and time to previous precipitation event was tested using a t-test of means. The null hypothesis that the state classification on the event conditions were independent was rejected if the p-value resulting from the t-test was less than 0.10.

## 2.5 Evaluating Scenario Variation

Since this study relied on evaluating the differences between paired scenarios to assess watershed capacitance, we needed a way to evaluate the practical "significance" of differences between model outputs. Doing so requires some means of assessing the model's sensitivity to differences in the input parameters. In deterministic models, the typical means of assessing model sensitivity is parameters is to select a range of values for parameterization that represent the uncertainty in the parameters (for example in hydraulic conductivity, which is often estimated with much uncertainty) for the site, and running multiple realizations of the simulation using different combinations of the parameters' values. In deterministic models any particular change in an input parameter will result in a change in the output model result, but small differences in modeled results may have little practical meaning. Therefore, the goal of sensitivity analysis is usually to input a wide range of parameter values to explore how much the modeled output responds. Given the computational resources (see section 2.2.6) needed to run one simulation for the domain with ParFlow, this was not a practical approach. Although the computational intensity of running ParFlow simulations makes parameter sensitivity testing impractical, the changed parameters between the nine scenarios tested can be thought of as tests on the sensitivity of the entire site that result in a range of order-of-magnitude variability associated with stormwater management techniques. The level of variation in the event-based runoff volumes between the range of parameterizations for the nine scenarios compared to the variation observed in event-based volumes from the empirical monitoring data from the RiverSmart Washington program for the site provides one way of evaluating the sensitivity of the site to the scenarios' changes and the relevance of the magnitudes of difference in performance between the scenarios. If the differences between the modeled output are not large enough to exceed the amount of variation that is seen in the monitored data given a particular rain event depth, and antecedent conditions, then the differences we would expect to see between the scenarios might not be observable in reality.

Total event precipitation is usually considered the most important control in assessing performance variation across scenarios. To capture variation of the runoff ratio conditional on total event depth, we calculated the absolute width of the confidence percentile intervals estimated from the regression of the total event runoff volume on the total event precipitation event from the monitored precipitation and flow data from the summer months of the pre-GI period (March – August 2010). In addition to the effect of total event precipitation, two important controls were included in the regression of total event runoff volume on the total event precipitation: the length of time between each rain event and the previous rain event, and the depth of the previous rain event. These two parameters were included to control for the effects of antecedent wetness conditions that influences the amount of volume generated from the site in a given rainfall event. **Equation 3** shows the regression specification:

$$volume\,mitigated_{m,t} = \beta_{0,m} + \beta_{1,m}\,prcp_t + \beta_{2,m}\,intertime_t + \beta_{3,m}\,prcp_{t-1} + e_{t,m} \qquad [3]$$

where $volume\,mitigated_{m,t}$ represents the volume of runoff mitigated by scenario *m* during event *t* compared to the modeled base case runoff during the event *t* ($m^3$); $prcp_t$ is the total depth of precipitation during event *t* (mm), $intertime_t$ is the inter-event period in hours between start of event *t* and the end of the previous event *t-1*, $prcp_{t-1}$ is the total depth of precipitation during the previous event *t-1*, $\beta_m$ are the coefficients estimated from linear regression for scenario *m*, and $e_{t,m}$ is the error. Following the estimation of the coefficients through linear regression, the models were used to predict the linear relationship of the effect of precipitation depth from zero to 50 mm, holding the interevent period and the previous rainfall event depth constant. The interevent period was held at the mean interevent period between all events during the modeled period (57.3 hours) and depth of the previous rainfall event was held at the mean rainfall event depth during the modeled period (7.8 mm). Holding the interevent period and the depth of the previous rainfall event constant allowed us to examine estimates of uncertainty conditional on varying the event *t*'s total rainfall depth.

The confidence interval represents the area in which the 'true' mean runoff volume is likely to reside, and takes into account the number of observations available in the range. The confidence interval for the slope of the regression line depends on the standard error of the sampling distribution of the slope. It is therefore is nonlinear in width, generally shorter when more observations are available, and larger when observations are scarcer. The width of the confidence interval was calculated by taking the difference in the upper confidence interval limit and the lower confidence interval limit. Confidence interval upper and lower limits were determined by several confidence levels: 95%, 90%, and 85%.

If the mean differences between the scenarios' total event runoff volumes is greater than the width of the confidence interval, conditional on the total event depth, this is an indication that the magnitude of the difference between the two scenarios might be large enough to attribute to outside the normal "noise" range of the PRE_GI monitoring data. For example, the simulated runoff volumes per event for GI_ROW and PRE_GI are differenced. This difference is then regressed on the precipitation depths for each event. The resulting estimated slope for the regression represents the mean expected difference in volume between these two scenarios at a given precipitation event depth. If this expected difference is greater than the width of the confidence interval observed from the monitored data, this indicates that that difference is outside the bounds of confidence associated with the noise of monitored data, and the difference may be noticeable.

# 3 RESULTS AND DISCUSSION

## 3.1 Six-month Flow Duration Curve Comparison

FDCs comparing scenarios are shown in **Figure 6.** Comparisons of the full distribution of flows, as well as zoomed-in insets of the maximum 1% of flows for each of the scenarios are depicted. A qualitative evaluation of the FDCs shows that among spatial configuration paired scenarios the greatest variation was observed between paired scenarios GI_ROW and GI_ROOF. GI_DRY/GI_WET and IS_DRY/IS_WET exhibited very small differences, both with the high flow accumulation properties treated (GI_WET and IS_WET) scenarios with lowered peak flows. The small differences in peaks cannot be clearly attributed to spatial configuration however, because the property-specific conditions of the site did not result in perfectly equal treated/removed areas between the DRY and WET scenarios; the WET scenarios had slightly higher amounts of impervious area treated/removed (**Table 4**). The least variation was observed between GI_DRY and IS_DRY, and GI_WET and IS_WET. These comparisons compare the effects of increasing hydraulic conductivity by 1 – 6 orders of magnitude in the top four layers of the domain.

The FDCs show that the only scenario to have a maximum peak flow clearly above that of the PRE_GI case is IS_MAX, the scenario that has 36.5% more impervious surface area than the PRE_GI case. All scenarios maintained the PRE_GI hydraulic conductivity and porosity values for the burned in pipe in the main ROW to represent unpressurized pipe flow in the site's storm drain system. Therefore, we expected GI_ROW, which treats the areas surrounding the burned in pipe, to increase low flow frequencies through gradual infiltration from the treatment areas to the burned in pipe. Instead, we observed decreased low flow frequencies compared to PRE_GI. This is evidence that the high pressure heads in the burned in pipe actually infiltrated out into the GI treatment areas in this spatial configuration, decreasing the low flow frequencies of GI_ROW overland flow at the monitoring point. Overall however, minimal differences between paired spatial configurations suggests that the capacitance of the study site sewershed is not limited.

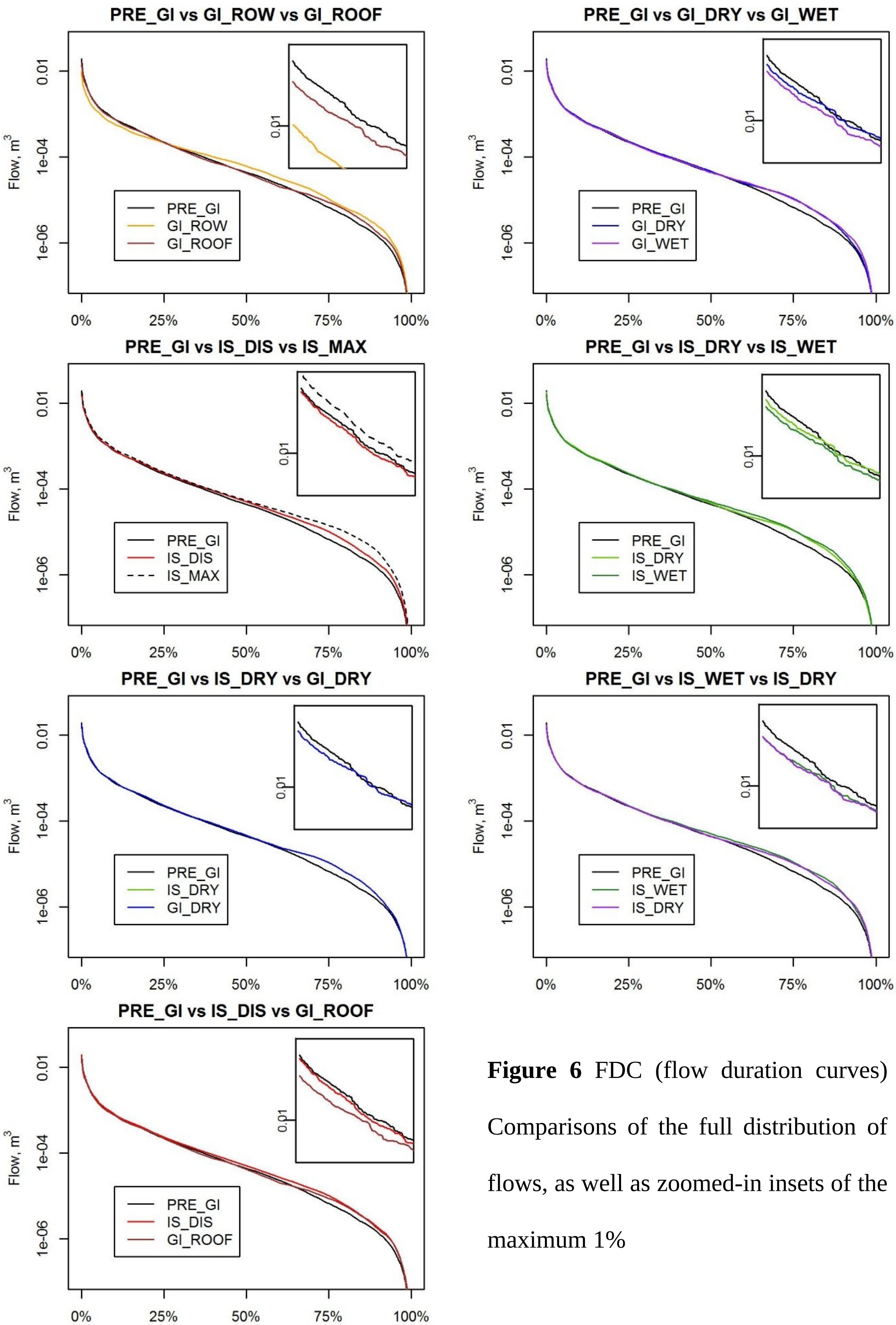


**Figure 6** FDC (flow duration curves) Comparisons of the full distribution of flows, as well as zoomed-in insets of the maximum 1%

## 3.2 Event-based analyses

The maximum runoff mitigation efficacies ($E_{S_{i,j}}$) of the scenarios over the PRE_GI case scenario ranged from 13.7 mm/m$^2$ treated area (IS_DRY) to 15.0 mm/m$^2$ treated area (GI_ROOF). The mean $E_{S_{i,j}}$ ranged from -1.05 mm/m$^2$ (more runoff was generated in IS_WET compared to the PRE_GI case) to 1.89 mm/m$^2$ (GI_WET). Plots of $E_{S_{i,j}}$ by the event total precipitation depths are shown in **Figure 7.** On average, no significant differences associated with spatial configuration are observed between treated (GI_WET and GI_DRY) or removed (IS_WET and IS_DRY) rooftop imperviousness. There is an observable difference between the performance of GI_ROW and GI_ROOF however, with each m$^2$ of GI in the GI_ROW case intercepting more runoff on average than the GI_ROOF case. Since GI_ROW was the spatial configuration with retrofits placed in high accumulation areas, this negates the expected response of a capacity constrained sewershed, where infiltration in high accumulation areas would be expected to perform less efficiently in larger precipitation events. **Figure 7** shows that when efficiency *Es* is regressed on precipitation depth, the slope of the regression line is steeper for GI_ROW than it is for GI_ROOF. This further demonstrates that as precipitation depth increases, the differential efficiency of the high accumulation configuration increased more quickly over the base scenario than the low accumulation configuration.

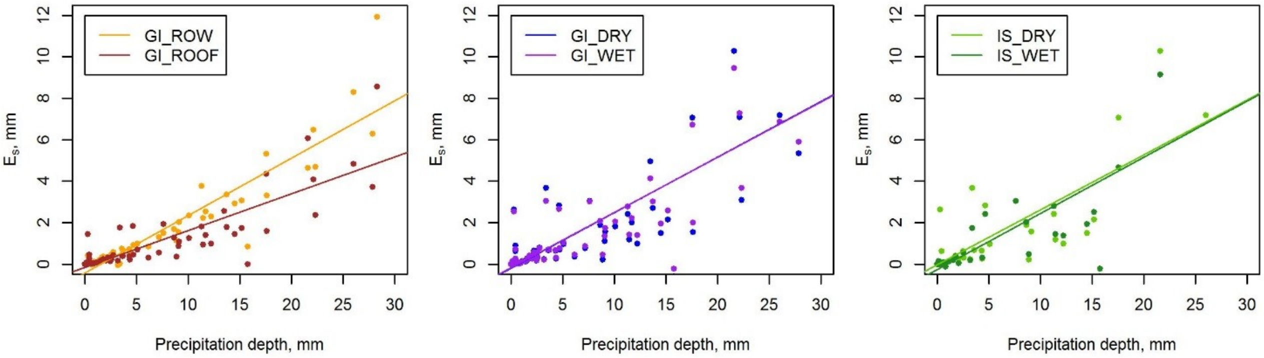


**Figure 7.** Calculated scenario efficacy ($E_s$) per square meter of treated/removed impervious area.

**Figure 8** shows box plots of the groups resulting from the classifications based on **Equation 2**.

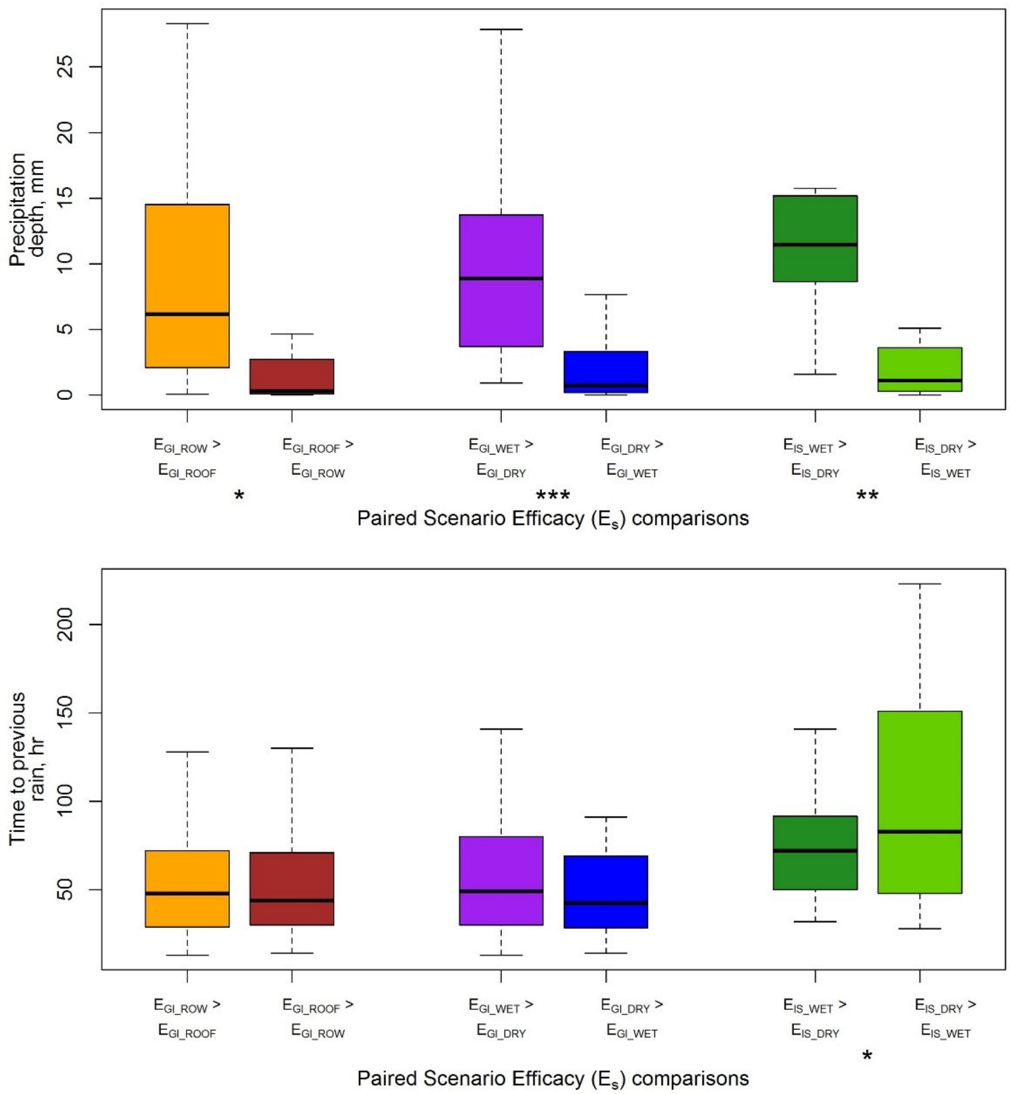


**Figure 8.** Paired spatial configuration scenarios efficacy comparisons and dependence on total event precipitation depth and time to previous precipitation event. *p<0.10; **p<0.05; ***p<0.0001

T-tests showed that the scenario with greater efficacy of each of the paired spatial configurations depended on the event's total precipitation depth ($p$ = 0.058, 0.00017, 0.0021, for GI_ROW/B, GI_DRY/B, and IS_DRY/B, respectively). During larger events, spatial configuration scenarios where imperviousness located in high flow accumulation areas of the sewershed was removed/treated were found to be more effective in reducing runoff volumes than spatial configuration scenarios located in low flow accumulation areas of the sewershed. The t-test for spatial efficacy's dependence on the inter-event period was only marginally significant ($p$ = 0.095) between the IS_DRY and IS_WET scenarios. This statistically significant result indicates that when events occur soon after a previous precipitation event, the spatial configuration where imperviousness is removed from high flow accumulation (WET) areas will perform better than the spatial configuration where imperviousness is removed from low flow accumulation (DRY) areas.

In conclusion, along with the FDC analysis, the results of both the linear dependence of $E_s$ on event precipitation depth and the more effective spatial configurations' dependence on event precipitation depth and time to previous event support the conclusion that the case study site is not capacity constrained. Statistical tests of paired WET/DRY scenarios provided evidence that interventions (treatment or removal) located at high flow accumulation areas of the sewershed are more effective than interventions located at low flow accumulation areas under wetter conditions. This indicates that the interventions located in high flow accumulation areas are capturing not only their direct contributing areas but also some upslope area. Had the sewershed been capacity constrained, we would have expected interventions located in high flow accumulation areas to perform worse under wetter conditions, when indirect shallow subsurface flows from upslope areas would have impeded the intervention to regain capacity to mitigate its own contributing area.

## 3.3 Variation in Observed and Simulated Scenarios' Flows

**Figure 9a** shows the difference between the runoff volumes for PRE_GI case and each of the scenarios, compared with the widths of the 95%, 90% and 75% confidence intervals of the estimated regression of runoff volume on precipitation depth. None of the scenarios exhibit a large enough difference from the PRE_GI case to exceed the level of noise in the monitoring data at the 90% - 95% confidence levels. Only the difference in runoff volume from one scenario, GI_ROW approaches the level of noise in the monitoring data at the 75% confidence level. Even the relatively dramatic increase in site imperviousness from 23,375 $m^2$ to 31,900 $m^2$ (36% increase) between PRE_GI and IS_MAX did not result in a large enough difference to cross the barrier of noise in the monitoring data.

Of all the combinations of scenarios simulated in this study, the maximum difference in mean event runoff volume was between IS_MAX (maximum allowable impervious surface developed) and GI_ROW (all ROW surface area treated with GI). These configurations and parameterizations led to a performance difference that just barely crosses the width of the 90%

confidence interval for the monitored data (**Figure 9b**).

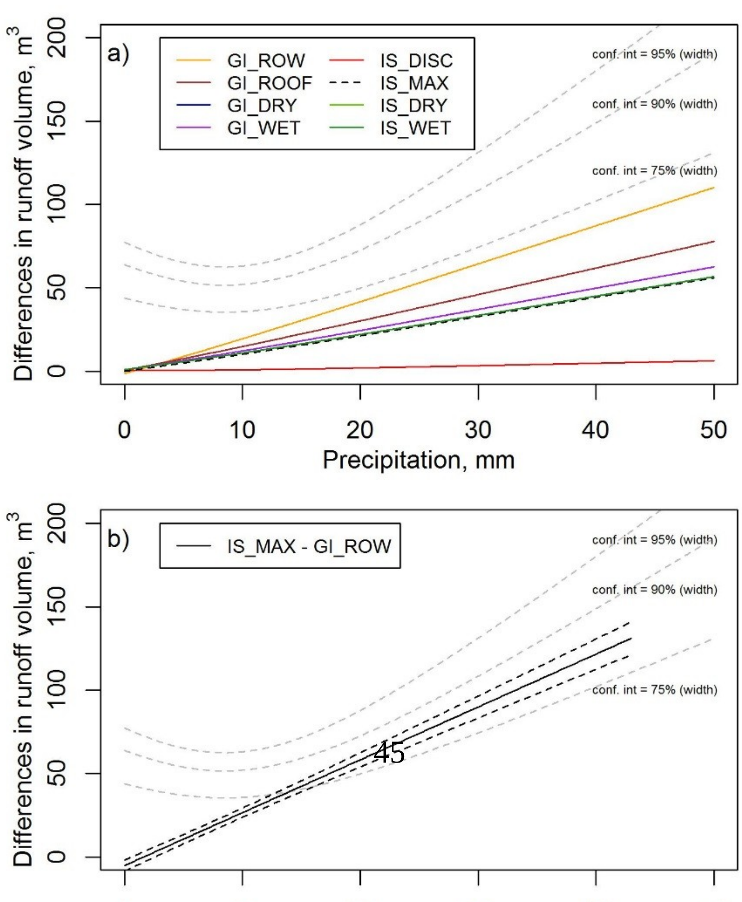

**Figure 9. a)** Comparisons of differences in runoff volume between each alternative scenario with the widths of the 75%, 90%, and 95% confidence intervals of difference in runoff volume's estimated dependence on precipitation depth (gray dashed lines). Confidence intervals were estimated from linear models of runoff volume regressed on precipitation depth, inter-event period, and depth of previous rainfall event (See **Equation 3**) **b)** Comparisons of differences in runoff volume between maximum treatment difference scenarios, IS_MAX and GI_ROW, with the widths of the 75%, 90%, and 95% confidence intervals of difference in runoff volume's estimated dependence on precipitation depth (gray dashed lines). The 95% confidence interval of the modeled difference in runoff volume between IS_MAX and GI_ROW is shown with black dashed lines.

## 4 CONCLUSIONS

The specifications of hydraulic conductivity and porosity used in this study, as well as the boundary conditions for the subsurface did not result in evidence of limited watershed capacitance. Therefore, we characterized this medium density, residential sewershed as having "high capacitance." For the six-month simulation period of this study, there was no evidence that treatments located in high flow-accumulation areas were less effective than treatments located in low flow-accumulation areas. This was shown to be the case because areas of high accumulation were not only intercepting their designated treatment areas during the event, but also intercepting upland flows near the ends of the precipitation event period. For example, there was very little accumulation of saturation or positive pressure head between precipitation events. In a low capacitance situation, we would have expected to see decreased effectiveness of treatment scenarios in higher accumulation areas under wetter conditions. We do acknowledge however that the year selected for our simulations was chosen because it was a close to average precipitation year. Different capacitance patterns could have be observed for the site under greater precipitation, when the site infiltration conditions could become more limiting.

It was also shown that while increased hydraulic conductivity from impervious to either green infrastructure or native soil levels increased watershed capacitance, there were no observable differences in capacitance between green infrastructure vs native soil (e.g.: between GI_DRY and IS_DRY). This finding may be related to the above finding in that the differences in hydraulic conductivity between native soil and GI may both not be constraining factors in watershed capacitance. Instead, the differences between paired spatial configuration scenarios (e.g.: between GI_DRY and GI_WET) resulted in more observable differences. The site is more sensitive to changes in spatial configuration than changes in hydraulic conductivity, at least when the changes are only applied to only 7-9% of the site. If more of the site's hydraulic conductivity were changed however, there is some evidence that indicates that differences in runoff volume would be more observable. There was evidence that differences in runoff volume increased as the total treated area increased. The largest difference between paired spatial configuration scenarios was observed between GI_ROW and GI_ROOF, which treated 14.2% and 15.6% of the site's impervious surface area, respectively, which was 5-7 percentage points greater than the treated areas in the paired scenarios GI_DRY/GI_WET (7.3%/9.2%) and IS_DRY/IS_DRY (7.3%/9.2%).

Lastly, this study developed a way of contextualizing the significance of magnitudes of differences observed between different scenarios. Given the amount of variation and noise present in monitored pipe flow data for the study site, only the differences in capacitance between IS_MAX and GI_ROW resulted in a difference large enough to exceed level of variation associated with 90% confidence interval from the observed flow data. The difference in impervious surface between these two scenarios was 30 percentage points. The difference between the PRE_GI and GI_ROW scenarios was large enough to exceed the level of variation associated with the 75% confidence interval. No other pairs of scenarios exceeded the level of variation in the monitored data.

There are several practical implications of this research. First, the spatial configuration of green infrastructure is an important consideration when deciding between treating ROW or dispersed treatments on private property within sewersheds of this development density. Treatment of ROW areas with GI is more effective than treatment of private roof areas because such treatment has the capacity to intercept more upslope areas. Based on topography, alleys and the ROW have the largest contributing area in the sewershed since they are located at the lowest areas of the site. However, our model represents each GI facility and its corresponding contributing area (the areas that were designed to be intercepted by the GI facility) as the weighted average of the GI and the porosity and hydraulic conductivity of its designed contributing area. Therefore, any additional interception by the GI facility from further upland areas come from either delayed surface runoff or shallow subsurface flow. This additional interception of upslope areas are evidenced by the downslope interventions increasing in effectiveness as wetness increases, and would only be possible if the GI receiving area was still had the capacity to intercept this additional flow.

Second, within residential sewersheds of this development density, a 50% property treatment rate does decrease runoff volumes and peaks compared to not doing anything, but spatial configuration is not important. Therefore, when either designing a voluntary residential GI program, or an impervious surface removal program (e.g.: vacant home demolition), spatial configuration of treatment properties will not make a difference in overland flow mitigation.

Third, a combination of variation and measurement noise in pipe flow monitoring results in a barrier to the detection of potential differences attributed to site change. This applies to both increases in imperviousness of up to 15 percentage points, and treatment/removal of imperviousness of up to 30 percentage points. This study showed that only a decrease of 30 percentage points of imperviousness resulted in a detectable change in response compared to the amount of variation and measurement noise in pipe flow monitoring data. This 30-percentage point decrease in imperviousness included both treating the ROW and a portion of building footprints, compared to the maximum allowable imperviousness for each property, highlighting the importance of residential participation in measurable mitigation of overland flows from urban sewersheds. This finding, for in-pipe flows monitored from a small urban sewershed, is in contrast to previous studies (eg: *Walsh et al.*, 2012) that have shown large changes in the hydrologic regime between catchments that have small differences in percent directly connected impervious surface. This study differs in several important ways. First, the sewershed studied in this research is much smaller (0.05 $km^2$) than many previously studied urban catchments. Second the site is primarily composed of developed, urban-use ‘pervious’ areas, which typically have much lower hydraulic conductivity and are more compacted than undeveloped ‘pervious’ areas. Theory suggests that these two characteristics would result in more difficulty in detection of the effects of small differences of site imperviousness or impervious surface connectivity, since the overland flow response would tend to dominate compared to larger catchments having large areas of undeveloped land.

The problem of detectable change and noisy empirical data may also have a regulatory implication. The site used in this study is served by a separate sewer system designed to only convey wet-weather flows and expected to have zero baseflow during dry weather. The selection of the monitoring technology for the site, ultrasonic level sensors to measure stage height and the subsequent rating curve developed to translate stage height to flow, may not have consistently and reliably measured runoff response under these conditions. Additional noise may have been introduced to the site through inputs not related to precipitation, such as lawn watering and car-washing in the neighborhood. Although empirical monitoring data analysis is typically held as the “gold standard” of experimental design, this study has shown ways that modeling can help fill in holes in understanding urban stormwater management, providing a way to “control” site conditions to conduct experiments about specific hydrological behaviors.

## ACKNOWLEDGEMENTS AND DATA

We would like to thank Steve Saari (Washington DC Department of Energy and the Environment) and Brad Udvardy (LimnoTech) for providing data from the RiverSmart Washington Program. The study utilized computational resources provided through the NSF’s Extreme Science and Engineering Discovery Environment (XSEDE) through the project “Multiscale surface-subsurface modeling of the Baltimore region” (TG-EAR130027). Simulations were conducted on Stampede at the Texas Advanced Computing Center. Modeling benefitted greatly from discussion with Michael Barnes, Elvis Andino, and Andy Miller (UMBC). The data used to produce the results of this study are available at: https://knb.ecoinformatics.org/#view/knb.1256.1 T. Lim's time was supported by a doctoral fellowship from the University of Pennsylvania's Department of City and Regional Planning. C. Welty's time was supported in part by US EPA grant R835555 and NSF grants CBET-1058038 and EAR-1427150.

## REFERENCES

Ahiablame, L. M., B. A. Engel, and I. Chaubey (2013), Effectiveness of low impact development practices in two urbanized watersheds: Retrofitting with rain barrel/cistern and porous pavement, *J. Environ. Manage.*, *119*, 151–161, doi:10.1016/j.jenvman.2013.01.019.

Ajami, H., J. P. Evans, M. F. McCabe, and S. Stisen (2014), Technical Note: Reducing the spin-up time of integrated surface water–groundwater models, *Hydrol Earth Syst Sci*, *18*(12), 5169–5179, doi:10.5194/hess-18-5169-2014.

Arnold, C. L., and C. J. Gibbons (1996), Impervious Surface Coverage: The Emergence of a Key Environmental Indicator, *J. Am. Plann. Assoc.*, *62*(2), 243–258, doi:10.1080/01944369608975688.

Ashby, S. F., and R. D. Falgout (1996), A Parallel Multigrid Preconditioned Conjugate Gradient Algorithm for Groundwater Flow Simulations, *Nucl. Sci. Eng.*, *124*(1), 145–159.

Barnes, M. L., C. Welty, and A. J. Miller (2015), Global Topographic Slope Enforcement to Ensure Connectivity and Drainage in an Urban Terrain, *J. Hydrol. Eng.*, *0*(0), doi:10.1061/(ASCE)HE.1943-5584.0001306.

Bhaskar, A., C. Welty, R. M. Maxwell, and A. J. Miller (2015), Untangling the effects of urban development on subsurface storage in Baltimore, *Water Resour. Res.*, *51*(2), 1158–1181, doi:10.1002/2014WR016039.

Bhaskar, A. S., C. Jantz, C. Welty, S. A. Drzyzga, and A. J. Miller (2016a), Coupling of the Water Cycle with Patterns of Urban Growth in the Baltimore Metropolitan Region, United States, *JAWRA J. Am. Water Resour. Assoc.*, *52*(6), 1509–1523, doi:10.1111/1752-1688.12479.

Bhaskar, A. S., D. M. Hogan, and S. A. Archfield (2016b), Urban base flow with low impact development, *Hydrol. Process.*, n/a-n/a, doi:10.1002/hyp.10808.

Burszta-Adamiak, E., and M. Mrowiec (2013), Modelling of green roofs' hydrologic performance using EPA's SWMM, *Water Sci. Technol.*, *68*(1), 36, doi:10.2166/wst.2013.219.

Chen, Y., S. D. Day, A. F. Wick, and K. J. McGuire (2014), Influence of urban land development and subsequent soil rehabilitation on soil aggregates, carbon, and hydraulic conductivity, *Sci. Total Environ.*, *494–495*, 329–336, doi:10.1016/j.scitotenv.2014.06.099.

Condon, L. E., and R. M. Maxwell (2014), Feedbacks between managed irrigation and water availability: Diagnosing temporal and spatial patterns using an integrated hydrologic model, *Water Resour. Res.*, *50*(3), 2600–2616, doi:10.1002/2013WR014868.

Davis, A. P. (2007), Field Performance of Bioretention: Water Quality, *Environ. Eng. Sci.*, *24*(8), 1048–1064, doi:10.1089/ees.2006.0190.

Davis, A. P. (2008), Field Performance of Bioretention: Hydrology Impacts, *J. Hydrol. Eng.*, *13*(2), 90–95, doi:10.1061/(ASCE)1084-0699(2008)13:2(90).

DDOE, FORCE, and LimnoTech (2011), Monitoring Report: Pre-Implementation Stormwater Volume Monitoring for Large Scale Low Impact Development Implementation,

Driscoll, C. T., C. G. Eger, D. G. Chandler, C. I. Davidson, B. K. Roodsari, C. D. Flynn, K. F. Lambert, N. D. Bettez, and P. M. Groffman (2015), *Green Infrastructure: Lessons from Science and Practice*, Science Policy Exchange.

Dunne, T., T. R. Moore, and C. H. Taylor (1975), Recognition and Prediction of Runoff-Producing Zones in Humid Regions, *Hydrol. Sci. - Bull.*, *20*(3), 305–327.

Emerson, C. H., and R. G. Traver (2008), Multiyear and Seasonal Variation of Infiltration from Storm-Water Best Management Practices, *J. Irrig. Drain. Eng.*, *134*(5), 598–605, doi:10.1061/(ASCE)0733-9437(2008)134:5(598).

Endreny, T., and V. Collins (2009), Implications of bioretention basin spatial arrangements on stormwater recharge and groundwater mounding, *Ecol. Eng.*, *35*(5), 670–677, doi:10.1016/j.ecoleng.2008.10.017.

Gilroy, K. L., and R. H. McCuen (2009), Spatio-temporal effects of low impact development practices, *J. Hydrol.*, *367*(3–4), 228–236, doi:10.1016/j.jhydrol.2009.01.008.

Gobel, P. et al. (2004), Near-natural stormwater management and its effects on the water budget and groundwater surface in urban areas taking account of the hydrogeological conditions, *J. Hydrol.*, *299*(3–4), 267–283, doi:10.1016/j.jhydrol.2004.08.013.

Hamel, P., E. Daly, and T. D. Fletcher (2013), Source-control stormwater management for mitigating the impacts of urbanisation on baseflow: A review, *J. Hydrol.*, *485*, 201–211, doi:10.1016/j.jhydrol.2013.01.001.

HSA, Inc (2012), *Data Report for RiverSmart Washington Project- Lafayette*, Washington DC.

Kollet, S. J., and R. M. Maxwell (2008), Capturing the influence of groundwater dynamics on land surface processes using an integrated, distributed watershed model, *Water Resour. Res.*, *44*(2), W02402, doi:10.1029/2007WR006004.

Lee, J., K. Hyun, and J. Choi (2013), Analysis of the impact of low impact development on runoff from a new district in Korea, *Water Sci. Technol.*, *68*(6), 1315, doi:10.2166/wst.2013.346.

Li, H., L. J. Sharkey, W. F. Hunt, and A. P. Davis (2009), Mitigation of Impervious Surface Hydrology Using Bioretention in North Carolina and Maryland, *J. Hydrol. Eng.*, *14*(4), 407–415, doi:10.1061/(ASCE)1084-0699(2009)14:4(407).

Lim, T. C. (2016), Predictors of urban variable source area: A cross-section analysis of urbanized catchments in the united states, *Hydrol. Process.*, n/a-n/a, doi:10.1002/hyp.10943.

Loperfido, J. V., G. B. Noe, S. T. Jarnagin, and D. M. Hogan (2014), Effects of distributed and centralized stormwater best management practices and land cover on urban stream hydrology at the catchment scale, *J. Hydrol.*, *519*, 2584–2595, doi:10.1016/j.jhydrol.2014.07.007.

Machusick, M. D. (2009), The Observed Effects of Stormw ater Infiltration on Groundwater, Villanova University, May.

Maimone, M., D. E. O'Rourke, J. O. Knighton, and C. P. Thomas (2011), Potential impacts of extensive stormwater infiltration in Philadelphia, *Environ. Eng. Appl Res Pract.*, *14*.

Maxwell, R. M. (2013), A terrain-following grid transform and preconditioner for parallel, large-scale, integrated hydrologic modeling, *Adv. Water Resour.*, *53*, 109–117, doi:10.1016/j.advwatres.2012.10.001.

Maxwell, R. M. et al. (2016), ParFlow User's Manual,

Miles, B., and L. E. Band (2015), Green infrastructure stormwater management at the watershed scale: urban variable source area and watershed capacitance, *Hydrol. Process.*, *29*(9), 2268–2274, doi:10.1002/hyp.10448.

Mitchell, K. E. (2004), The multi-institution North American Land Data Assimilation System (NLDAS): Utilizing multiple GCIP products and partners in a continental distributed hydrological modeling system, *J. Geophys. Res.*, *109*(D7), doi:10.1029/2003JD003823.

Moglen, G. E., and S. Kim (2007), Limiting Imperviousness, *J. Am. Plann. Assoc.*, *73*(2), 161–171, doi:10.1080/01944360708976150.

Oleson, K. W. (2010), Technical Description of version 4.0 of the Community Land Model (CLM),

Page, J. L., R. J. Winston, D. B. Mayes, C. Perrin, and W. F. Hunt III (2015), Retrofitting with innovative stormwater control measures: Hydrologic mitigation of impervious cover in the municipal right-of-way, *J. Hydrol.*, *527*, 923–932, doi:10.1016/j.jhydrol.2015.04.046.

Palla, A., and I. Gnecco (2015), Hydrologic modeling of Low Impact Development systems at the urban catchment scale, *J. Hydrol.*, *528*, 361–368, doi:10.1016/j.jhydrol.2015.06.050.

Pennino, M. J., R. I. McDonald, and P. R. Jaffe (2016), Watershed-scale impacts of stormwater green infrastructure on hydrology, nutrient fluxes, and combined sewer overflows in the mid-Atlantic region, *Sci. Total Environ.*, *565*, 1044–1053, doi:10.1016/j.scitotenv.2016.05.101.

Qin, H., Z. Li, and G. Fu (2013), The effects of low impact development on urban flooding under different rainfall characteristics, *J. Environ. Manage.*, *129*, 577–585, doi:10.1016/j.jenvman.2013.08.026.

Schueler, T. (1994), The Importance of Imperviousness., *Watershed Prot. Tech.*, *1*(3), 100–111.

Seck, A., C. Welty, and R. M. Maxwell (2015), Spin-up behavior and effects of initial conditions for an integrated hydrologic model, *Water Resour. Res.*, *51*(4), 2188–2210, doi:10.1002/2014WR016371.

Shuster, W. D., and L. Rhea (2013), Catchment-scale hydrologic implications of parcel-level stormwater management (Ohio USA), *J. Hydrol.*, *485*, 177–187, doi:10.1016/j.jhydrol.2012.10.043.

Smith, B. K., J. A. Smith, M. L. Baeck, and A. J. Miller (2015), Exploring storage and runoff generation processes for urban flooding through a physically based watershed model, *Water Resour. Res.*, *51*(3), 1552–1569, doi:10.1002/2014WR016085.

University of Vermont (2011), High-Resolution Land Cover for Washington DC,

US EPA, O. of W. (2009), *Technical Guidance on Implementing the Stormwater Runoff Requirements for Federal Projects under Section 438 of the Energy Independence and Security Act*, Washington DC.

Valderrama, A., and L. Levine (2013), *Creating Clean Water Cash Flows: Developing Private Markets for Green Stormwater Infrastructure in Philadelphia*, NRDC.

Vienken, T., and P. Dietrich (2011), Field evaluation of methods for determining hydraulic conductivity from grain size data, *J. Hydrol.*, *400*(1–2), 58–71, doi:10.1016/j.jhydrol.2011.01.022.

Walsh, C. J., T. D. Fletcher, and M. J. Burns (2012), Urban Stormwater Runoff: A New Class of Environmental Flow Problem, *PLOS ONE*, *7*(9), e45814, doi:10.1371/journal.pone.0045814.

Zellner, M., D. Massey, E. Minor, and M. Gonzalez-Meler (2016), Exploring the effects of green infrastructure placement on neighborhood-level flooding via spatially explicit simulations, *Comput. Environ. Urban Syst.*, *59*, 116–128, doi:10.1016/j.compenvurbsys.2016.04.008.